Positive modulation of a Cys-loop acetylcholine receptor by an auxiliary transmembrane subunit

Thomas Boulin[1–3], Georgia Rapti[1–3,5], Luis Briseño-Roa[1–3,5], Christian Stigloher[1–3,5], Janet E Richmond[4], Pierre Paoletti[1–3] & Jean-Louis Bessereau[1–3]

Auxiliary subunits regulate the trafficking, localization or gating kinetics of voltage- and ligand-gated ion channels by associating tightly and specifically with pore-forming subunits. However, no auxiliary subunits have been identified for members of the Cys-loop receptor superfamily. Here we identify MOLO-1, a positive regulator of levamisole-sensitive acetylcholine receptors (L-AChRs) at the *Caenorhabditis elegans* neuromuscular junction. MOLO-1 is a one-pass transmembrane protein that contains a single extracellular globular domain—the TPM domain, found in bacteria, plants and invertebrates, including nonvertebrate chordates. Loss of MOLO-1 impairs locomotion and renders worms resistant to the anthelmintic drug levamisole. In *molo-1* mutants, L-AChR-dependent synaptic transmission is reduced by half, while the number and localization of receptors at synapses remain unchanged. In a heterologous expression system, MOLO-1 physically interacts with L-AChRs and directly enhances channel gating without affecting unitary conductance. The identification of MOLO-1 expands the mechanisms for generating functional and pharmacological diversity in the Cys-loop superfamily.

Auxiliary subunits are essential regulators of voltage- and ligand-gated ion channels. Over the past decade, a diverse set of structurally unrelated auxiliary subunits have been shown to regulate glutamate-gated AMPA and kainate receptors[1–9]. Stargazin, the founding member of the transmembrane AMPA receptor regulatory protein (TARP) family, has a major impact on AMPA receptor biology. It binds to receptors early in the biosynthetic pathway to promote their maturation, regulates their trafficking to the plasma membrane and controls their incorporation into postsynaptic scaffolds through interactions with PSD95. TARPs and NETO1/NETO2 also modulate the gating properties of AMPA and kainate receptors, respectively, explaining some of the discrepancies observed between native and recombinant receptors[5,7].

In contrast to the abundance of auxiliary subunits known to regulate glutamatergic receptors, no auxiliary subunits have so far been described for the large superfamily of Cys-loop ligand-gated ion channels, including GABA$_A$ and nicotinic acetylcholine receptors. Two ionotropic acetylcholine receptors (AChRs) mediate fast excitatory neurotransmission at *C. elegans* neuromuscular junctions. They can be distinguished by their specific pharmacologies[10]. The homomeric N-AChR is activated by nicotine and likely composed exclusively of ACR-16 α-subunits[11,12]. The heteromeric levamisole-sensitive AChR (L-AChR) is insensitive to nicotine but can be selectively activated by levamisole, a nematode-specific cholinergic agonist and anthelmintic drug[10,13]. Exposure to high concentrations of levamisole causes rapid muscle hypercontraction and death of wild-type animals. Genetic screens for mutations that confer resistance to levamisole in

C. elegans have identified five genes encoding L-AChR pore-forming subunits[14–17]: three α subunits (LEV-8, UNC-38, UNC-63) and two non-α subunits (UNC-29, LEV-1). In addition, three ancillary factors have been identified as indispensable proteins required for the proper biosynthesis and trafficking of these receptors[13,18,19]. More recently, functional reconstitution of L-AChRs in *Xenopus laevis* oocytes has confirmed the strict requirement for ancillary factors and the receptor's subunit composition[13]. Finally, three extracellular scaffolding proteins (LEV-9, LEV-10 and OIG-4) have been found to control the precise clustering of L-AChRs at postsynaptic sites through a network of direct molecular interactions[20–22].

To identify new genes involved in the regulation of L-AChR and, in particular, genes encoding possible auxiliary subunits, we performed a genetic screen for mutants with partially decreased sensitivity to levamisole. Here we demonstrate that *molo-1* (*modulator of levamisole receptor-1*) is an auxiliary subunit of the levamisole-sensitive acetylcholine receptor. *molo-1* encodes a previously uncharacterized single-pass transmembrane protein that colocalized with L-AChRs at neuromuscular junctions. Behavioral, pharmacological and electrophysiological assays showed that mutations in *molo-1* partially disrupted L-AChR function. However, reduced receptor function could not be explained by a defect in L-AChR expression or clustering at synapses, hence suggesting a direct effect of MOLO-1 on receptor activity. This was tested by expressing MOLO-1 with L-AChR in *Xenopus* oocytes, where we found that MOLO-1 physically interacted with L-AChR and increased L-AChR channel gating. Thus, MOLO-1 fulfils the criteria of a bona fide auxiliary protein.

Figure 1 The TPM domain-containing protein MOLO-1 is required for L-AChR function in muscle. (**a**) Percentage (mean ± s.e.m.) of paralyzed worms after overnight exposure to 0.6 mM levamisole. Transgenic *molo-1(kr100)* worms are rescued by the *molo-1* genomic fragment or the same *molo-1* genomic fragment in an artificial operon with an *SL2* (spliced leader 2)-*gfp* cassette. Expression of the *molo-1a* cDNA in muscle using the *Pmyo-3* promoter, but not expression in neurons using the *Prab-3* promoter, rescues the *molo-1* mutant phenotype. *N*, number of independent transgenic lines; >20 worms per line. (**b**) Thrashing rates in liquid of wild-type worms (112.6 ± 2.3 body bends per minute, *n* = 7, *N* = 34), *molo-1* mutants (76.9 ± 2.0 body bends per minute, *n* = 6 worms, *N* = 29 trials), *unc-29* mutants (59.0 ± 2.8 body bends per minute, *n* = 6, *N* = 26) and after expression of a GFP-tagged *molo-1a* cDNA in muscle cells alone (115.9 ± 2.9 body bends per minute, *n* = 5, *N* = 27). Mean ± s.e.m.; ANOVA; **P* < 0.01 versus wild-type and for the comparison between *molo-1(kr100)* and *unc-29(x29)*; NS, not significant, *P* = 0.36.

(**c**) *molo-1* exon-intron structure, *Mos1* transposon insertion sites (red triangles) and allele names. (**d**) The MOLO-1A and MOLO-1B splice isoforms differ only in their cytoplasmic regions (black rectangles). SP, signal peptide. (**e**) TPM domains are composed of four α-helices that flank a central β-sheet. The TPM domain of MOLO-1 is modeled on the basis of homology with the bacterial 2KW7 structure (see also **Supplementary Fig. 2**). α-helices (α1, α2, α3, α4), red; β-strands (β1, β2, β3, β4), yellow; loop regions, gray.
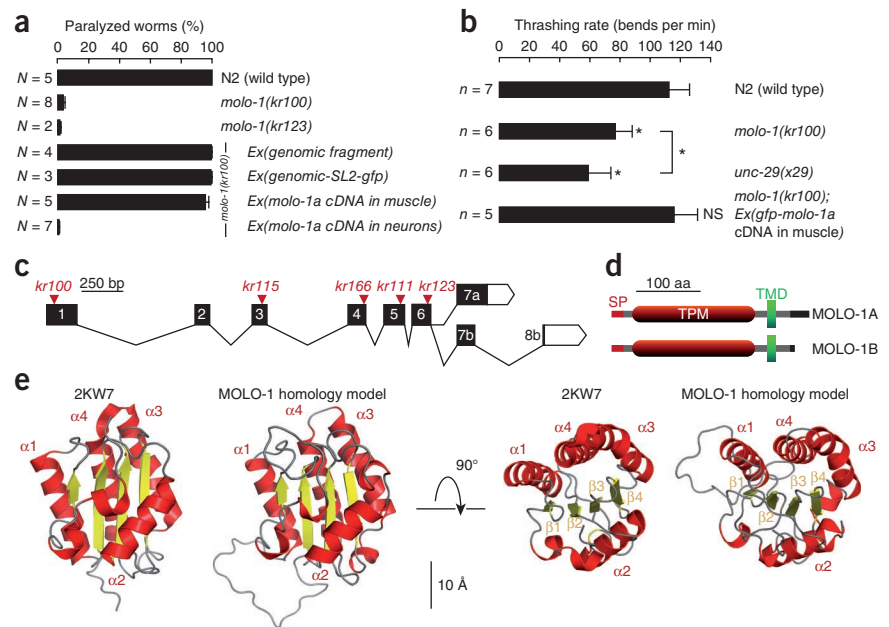
RESULTS

MOLO-1 is required for L-AChR function in muscle

To identify genes involved in the regulation of L-AChR function, we screened for mutants with decreased sensitivity to levamisole. Mutagenized worms were exposed to lethal concentrations of levamisole and resistant mutants isolated after 12 to 18 h. Transposon-based insertional mutagenesis was used to facilitate molecular cloning of the resulting mutants[23–25]. In the course of this screen, we retrieved five alleles of the uncharacterized gene *F09F7.1*, which we named *molo-1*. When exposed to high concentrations of levamisole, *molo-1* mutants initially became hypercontracted and paralyzed but recovered from the paralysis after 10 to 12 h, whereas the wild-type worms died. This levamisole resistance phenotype was fully penetrant and could be completely rescued with a PCR-amplified genomic DNA fragment containing only the *F09F7.1* open reading frame (**Fig. 1**). In addition to levamisole resistance, *molo-1* mutants displayed mild locomotory defects on agar plates. These defects were more severe in liquid media, where thrashing rates of *molo-1* mutants were significantly lower than those of the wild type but less reduced than those of *unc-29* mutants, which lack L-AChRs (**Fig. 1b**).

molo-1 encodes a single-pass transmembrane protein with a predicted N-terminal signal peptide followed by a TPM (TLP18.3/Psb32/MOLO-1) domain (PFAM PF04536, formerly known as DUF477) (**Fig. 1d**). *molo-1* is alternatively spliced, resulting in two proteins, MOLO-1A and MOLO-1B, which differ slightly in the C terminus (**Fig. 1c,d**). Six uncharacterized *molo-1* paralogs exist in *C. elegans*, and highly conserved *molo-1* orthologs are present in distantly related nematode species, in particular in human parasites such as *Ascaris* sp., *Loa loa* and *Brugia malayi*. Altogether, over 2,000 TPM domain-containing proteins have been detected in the sequenced genomes of bacteria, plants, protozoa and metazoans. In deuterostomes, TPM domains are present in hemichordates and in the cephalochordate amphioxus but are not obviously found in vertebrates

(**Supplementary Fig. 1** and **Supplementary Table 1**). To our knowledge, MOLO-1 is the first of these TPM-containing proteins to be functionally characterized in any metazoan.

The TPM domain is a small (~200 amino acids) globular domain that is almost always flanked by an N-terminal signal sequence and a C-terminal transmembrane domain (TMD) (1,341 of 1,351 sequences in the Pfam database). Although TPM domain–containing proteins differ widely at the level of their primary sequences, analysis of their secondary structures strongly suggests a conserved fold. Indeed, secondary structure prediction of representative members of TPM-containing proteins from 19 organisms revealed a notably conserved pattern (**Supplementary Fig. 1b**). The NMR structures of two prokaryotic TPM-containing proteins[26] (PDB 2KW7 and 2KPT) and the X-ray structure of the *Arabidopsis thaliana* protein AtTLP18.3 (ref. 27; PDB 3PVH) show that these domains consist of a central hydrophobic β-sheet, made of four β-strands, flanked by four or five amphiphilic α-helices (**Fig. 1e** and **Supplementary Fig. 2**). Using 2KW7 as a template, we built a three-dimensional homology model for the TPM domain of MOLO-1 (**Fig. 1e**). This model revealed a shared tertiary structure organization with diverging loops interconnecting the secondary structure elements. Notably, despite only 16% sequence identity, this model also identified in every α-helix a set of hydrophobic residues similarly oriented toward the β-sheet hydrophobic core (**Supplementary Fig. 2b**). These residues are generally conserved across phyla and likely contribute to the folding and stability of the TPM domain.

Loss of *molo-1* impairs L-AChR function but not expression

The phenotypes of *molo-1* mutants suggested that MOLO-1 is required for the function of L-AChRs. To test this hypothesis, we measured the electrophysiological response of voltage-clamped muscle cells to pressure-applied levamisole in wild-type and mutant animals[10]. In *molo-1* mutants, we observed an ~50% reduction in the peak current as compared to wild type (**Fig. 2a**). To assess the sensitivity
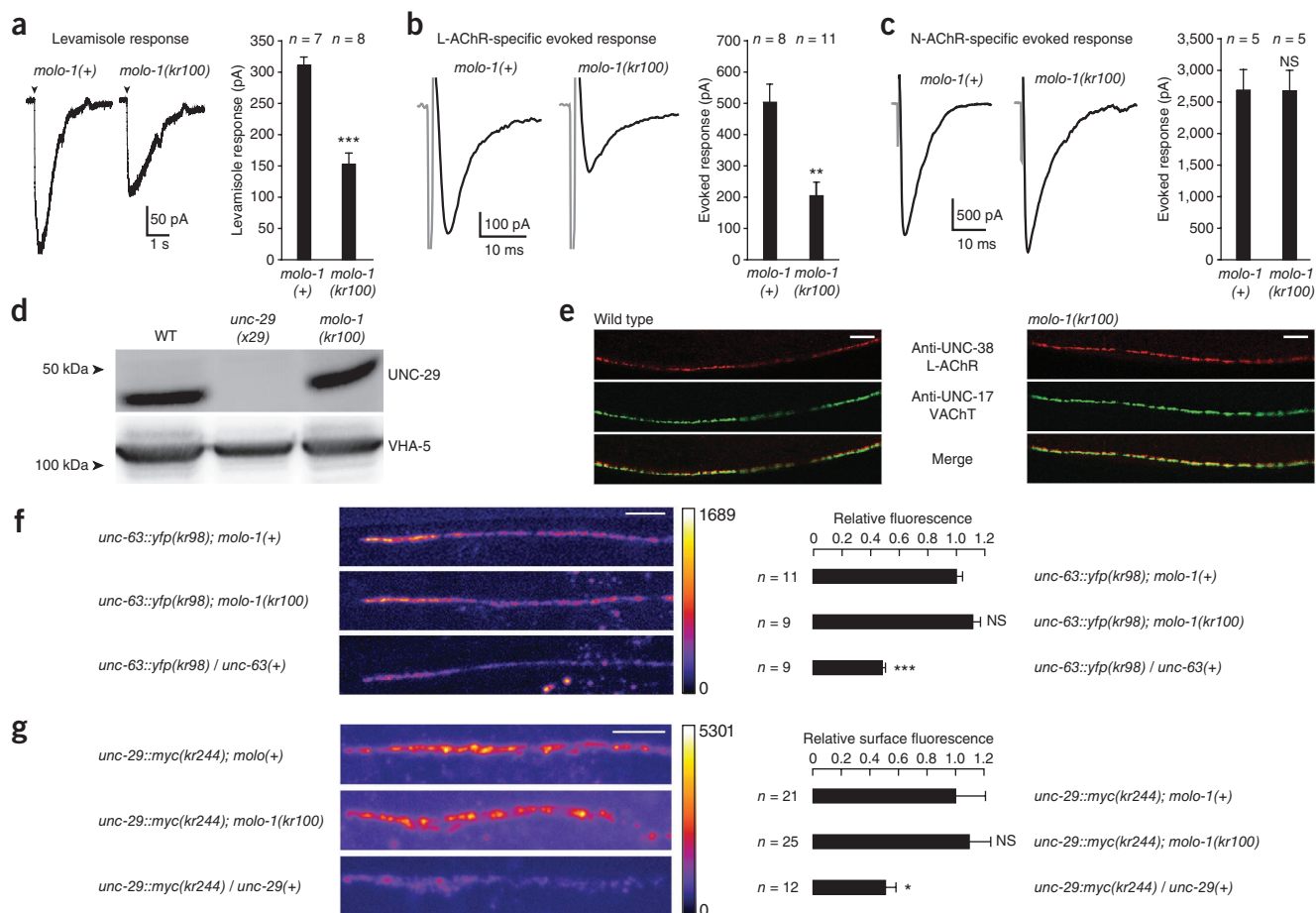
Figure 2 Loss of MOLO-1 specifically impairs L-AChR function without affecting receptor expression, trafficking or localization. (**a**) Peak currents evoked by 100-ms pressure application of 500 μM levamisole (arrowheads mark application onset). (**b**) L-AChR-dependent evoked synaptic responses in *molo-1(+)* and *molo-1* mutant worms, in an *unc-49(e407); acr-16(ok789)* double mutant background. (**c**) N-AChR-dependent evoked responses in *molo-1(+)* and *molo-1* mutant worms, recorded in an *unc-29(x29); unc-49(e407)* background. Stimulation artifacts are gray in **b,c**. (**d**) Western blot analysis of L-AChRs in wild-type worms (WT) and *molo-1* mutants. UNC-29 levels were normalized to VHA-5, the V0 α-subunit of the vacuolar proton-translocating ATPase (percentage of wild-type levels was $111 \pm 7\%$ ($n = 2$) in *molo-1(kr100)*; mean ± absolute deviation). (**e**) Detection of presynaptic cholinergic boutons (vesicular acetylcholine transporter (VAChT) staining) and L-AChR clusters in wild type and *molo-1* mutants. Anterior mid-body region; anterior is to the left, left is up. (**f**) Total synaptic content of L-AChR quantified with an UNC-63-YFP knock-in L-AChR subunit. (**g**) Surface detection of myc-tagged UNC-29 L-AChR subunits. Surface receptors were labeled with anti-myc-Cy3 injected into *unc-29::myc* knock-in worms. Pixel intensity is in arbitrary units in **f,g**. Anterior portion of the dorsal nerve cord; anterior is to the left, right is up. Pixel intensity in arbitrary units. Mean ± s.e.m.; n = number of worms; Student's t-test (except **g**, Kolmogorov-Smirnov test) *$P < 0.05$, **$P < 0.001$, ***$P < 0.0001$; NS, not significant. Scale bars, 10 μm.

of synaptic L-AChRs to the endogenous neurotransmitter acetylcholine, we measured evoked synaptic responses in *molo-1* mutants[10]. Although rise and decay times of L-AChR–specific evoked responses were indistinguishable from wild type, L-AChR-dependent synaptic peak currents were decreased by ~60% in *molo-1* mutants (**Fig. 2b**), consistent with the reduction of whole-cell L-AChR responses. This effect was specific for postsynaptic L-AChRs, as N-AChR- and GABA$_A$R-dependent postsynaptic responses remained unchanged in *molo-1* mutants (**Fig. 2c** and **Supplementary Fig. 3**). The fact that evoked responses mediated by N-AChRs were unchanged suggested that the decrease in L-AChR-dependent synaptic responses was not due to presynaptic defects in *molo-1* mutants (**Fig. 2c**). Taken together, these data argue that MOLO-1 specifically decreases the activity of postsynaptic L-AChRs.

The reduction of L-AChR currents could result simply from a decrease in receptor expression. To test this possibility, we assessed the overall content of receptors in wild type and in *molo-1* mutants by western blot analysis and observed no decrease in the total amount of

L-AChRs in *molo-1* mutants (**Fig. 2d** and **Supplementary Fig. 4a**). An alternative hypothesis would be that MOLO-1 is required for L-AChR trafficking to the plasma membrane. To test this hypothesis, we stained *molo-1* mutants with an antibody to the L-AChR subunit UNC-38. We found that receptors were still clustered at neuromuscular junctions of *molo-1* mutants (**Fig. 2e**). Although L-AChR cluster intensities appeared similar in wild type and mutants, we could not formally exclude a moderate difference in synaptic receptor content because immunostaining efficiency can vary for technical reasons. To accurately quantify receptors at synapses, we used a knock-in strain in which *yfp* was inserted into the genomic locus of *unc-63*, which encodes an essential L-AChR subunit[21]. There was no significant difference in receptor-associated fluorescence between wild-type and *molo-1* mutant worms (**Fig. 2f**). Because the maximum fluorescence decrease anticipated in *molo-1* is only ~50%, we assessed the sensitivity of our measurements by comparing the fluorescence in *unc-63::yfp* homozygous (two copies of the tagged locus) and heterozygous (one wild-type and one tagged allele)

Figure 3 MOLO-1 colocalizes with L-AChRs at synapses. (**a**) An artificial operon containing a *molo-1a* genomic fragment and a *gfp* cassette drives GFP expression in a subset of ventral nerve cord motor neurons (filled arrowheads), body wall (asterisks) and vulval muscle (vm). Dorsally projecting commissures (open arrowheads) can be seen at higher magnification. *Punc-122::gfp*, which labels coelomocytes (cc), was used as an injection marker. In left panel, anterior is to the left, left side is up. Right panel shows ventral mid-body region; anterior is to the left. Scale bars, 20 μm. (**b**) A muscle-expressed GFP–MOLO-1A fusion protein is localized to the nerve ring (nr) and ventral and dorsal cord (vnc and dnc, respectively) synapses. Confocal images of anesthetized worms (**a**,**b**). Asterisks, gut autofluorescence. (**c**) GFP–MOLO-1A colocalizes with L-AChRs at neuromuscular junctions. Mid-body region; anterior is to the left, left is up. (**d**) Colocalization of GFP-MOLO-1A with L-AChRs at neuromuscular junctions in *unc-49* (GABA_AR) *acr-16* (NAChR) double mutants. (**e**) GFP–MOLO-1A at the cell surface, labeled by injection of anti-GFP–Alexa 594 into the pseudocoelomic space of live worms expressing GFP–MOLO-1A. Anterior dorsal nerve cord; anterior is to the left, right is up. (**f**) Retention of GFP–MOLO-1A in intracellular compartments in *unc-29* mutants, which do not produce functional L-AChRs. Dashed lines, muscle cell outlines. Mid-body region; anterior is to the left, left is up. (**g**) Percentage of paralyzed worms after overnight exposure to 0.6 mM levamisole in transgenic *molo-1* worms expressing in muscle either the full length MOLO-1B, a HA–MOLO-1A chimera, a GFP–MOLO-1A chimera or a truncation lacking the cytosolic portion. Synaptic localization of tagged MOLO-1 variants is indicated at right. Red dots indicate data for individual transgenic lines. Mean ± s.e.m., *N* = number of independent lines; 30 worms per line. Scale bars, 10 μm, except in **a**.
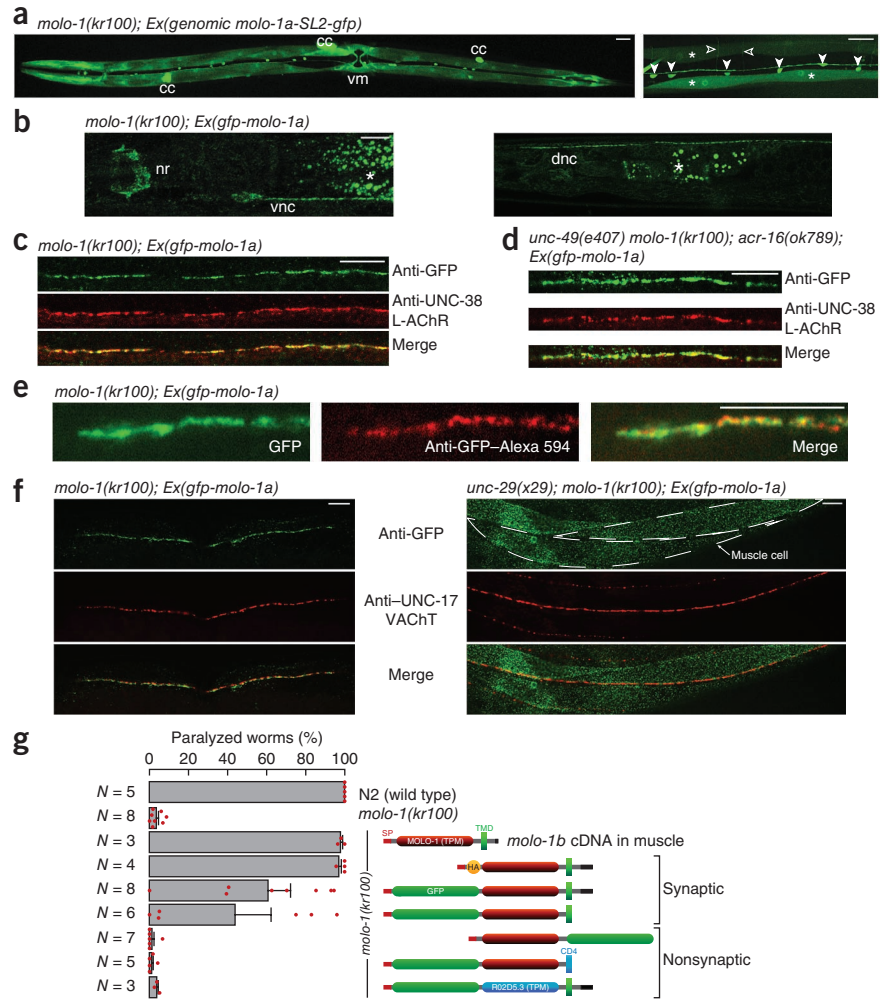
worms. Heterozygous worms clearly showed half the fluorescence of homozygotes, confirming the sensitivity of this approach (**Fig. 2f**).

Although these results indicated that the amount of L-AChRs present at synapses was not reduced in *molo-1* mutants, they do not demonstrate that these receptors are properly inserted in the postsynaptic plasma membrane. To quantify synaptic L-AChRs at the cell surface, we used *Mos*TIC genome engineering[28] to generate a *C. elegans* strain expressing an UNC-29 L-AChR subunit with an extracellular myc tag at its C terminus (**Fig. 2g** and **Supplementary Fig. 5**). Fluorescently labeled anti-myc antibodies injected into the pseudocoelomic cavity[29] of live *unc-29::myc* worms exclusively labeled receptors inserted in the plasma membrane. The staining pattern was clearly reminiscent of the one observed with L-AChR antibodies (**Fig. 2e**) or in the *unc-63::yfp* knock-in strain (**Fig. 2f**). Quantification showed no significant difference between wild-type and *molo-1* mutant worms, whereas we were able to detect a twofold difference in fluorescence relative to worms heterozygous for the *unc-29::myc* locus (**Fig. 2g**). Yet electrophysiological recordings in *unc-29::myc* strains confirmed that levamisole-evoked currents were reduced by ~50% in a *molo-1* mutant background (199 ± 15 nA versus 107 ± 7 nA; Student's *t*-test *P* = 0.0017; *n* = 4). Taken together, these results suggest that loss of *molo-1* decreases levamisole-sensitivity of *C. elegans* by decreasing the function of L-AChRs without affecting their expression, trafficking or synaptic localization.

MOLO-1 colocalizes with L-AChR at neuromuscular synapses

As MOLO-1 is not required for synaptic delivery of the L-AChRs, MOLO-1 might associate with L-AChRs to regulate their activity at the synapse. To identify in which tissues *molo-1* is required, we first analyzed its expression profile using a bicistronic reporter construct containing a 6.7-kb *molo-1* genomic DNA fragment followed by *gfp*. This transgene efficiently rescued the *molo-1* levamisole-resistance phenotype (**Fig. 1a**) and expressed GFP in body wall muscle, vulval muscle and a subset of ventral nerve cord motor neurons (**Fig. 3**). To identify the site of action of MOLO-1, we expressed the *molo-1a* cDNA under the control of muscle- and neuron-specific promoters (*Pmyo-3* and *Prab-3*, respectively). Expression of *molo-1a* in muscle but not neurons was sufficient to rescue the levamisole-resistance phenotype (**Fig. 1a**). Consistently, expression of MOLO-1A in muscle also rescued the locomotion defect of *molo-1* mutants (**Fig. 1b**), further demonstrating that MOLO-1 acts cell autonomously in muscle to regulate L-AChRs.

Next, we expressed an N-terminally tagged GFP–MOLO-1 fusion to analyze the subcellular localization of MOLO-1 in muscle. This protein rescued the *molo-1* mutant phenotypes (**Figs. 1b** and **3g**) and formed distinct clusters along the ventral and dorsal nerve cords and in the nerve ring, a pattern reminiscent of L-AChR localization (**Fig. 3b**). Using an UNC-38 (L-AChR) antibody, we showed that GFP–MOLO-1A indeed colocalized with L-AChRs at neuromuscular junctions (**Fig. 3c**). Furthermore, by injecting

Figure 4 MOLO-1 and L-AChRs form a receptor complex *in vivo*. (**a**) A muscle-expressed, HA-tagged MOLO-1A fusion protein colocalizes with L-AChR at neuromuscular junctions. Anti-GFP labels L-AChRs expressed at neuromuscular junctions in the *unc-63::yfp(kr98)* knock-in strain. Anti-HA is used to label HA–MOLO-1A expressed in muscle in *Is(HA-molo-1a) (krIs45)* worms. Images are maximum-intensity projections of confocal stacks. Anterior mid-body region; anterior is to the left, left is up. Scale bar, 10 μm. (**b**) HA–MOLO-1 immunoprecipitates with L-AChR but not with N-AChR. L-AChR and N-AChR were immunoprecipitated (IP) from total membrane extracts by using GFP antibodies that bind the L-AChR subunit fusion (UNC-63–YFP) and the N-AChR subunit (ACR-16–GFP). A nonspecific band labeled by anti–UNC-29 in all samples served as a loading control.

unc-63::yfp(kr98); molo-1(kr100); Is(HA-molo-1a cDNA in muscle)

fluorescently labeled antibodies to GFP into live GFP–MOLO-1A–expressing worms, we demonstrated that GFP–MOLO-1A was in fact present at the cell surface (**Fig. 3e**).

These data suggested that MOLO-1 could associate with L-AChRs at neuromuscular junctions. To test whether MOLO-1 localization would depend on L-AChRs, we introduced the GFP–MOLO-1A fusion in an *unc-29(x29)* mutant background, which does not produce L-AChRs. In the absence of L-AChRs, GFP–MOLO-1A was retained in intracellular compartments and no longer localized to synapses (**Fig. 3f** and **Supplementary Fig. 6**). In contrast, inactivating the N-AChR ACR-16 and the GABA$_A$ receptor UNC-49, which are expressed in the same muscle cells, did not affect MOLO-1 localization (**Fig. 3d** and **Supplementary Fig. 6**). These results indicate that, although L-AChRs do not require MOLO-1 to localize at synapses, MOLO-1 is a synaptic protein that likely interacts with L-AChRs to be properly targeted to the membrane.

To identify which regions of the MOLO-1 protein are required for its targeting and function, we expressed a series of chimeric and deletion proteins in muscle (**Fig. 3g**). Expression of the alternative splice variant MOLO-1B that differs in the C-terminal end of MOLO-1 rescued *molo-1(kr100)* levamisole sensitivity. Likewise, removal of the entire cytoplasmic domain of GFP–MOLO-1A did not affect its localization or functionality. When we deleted its TMD and cytoplasmic end, MOLO-1–GFP was efficiently secreted from muscle cells, as based on the strong fluorescence signal observed in coelomocytes (**Supplementary Fig. 6d**), but was not retained at synapses and did not rescue the mutant phenotype. When we fused the extracellular portion of GFP–MOLO-1A with a heterologous TMD (human CD4), this chimeric protein failed to localize to synapses and did not rescue the *molo-1* phenotype. Finally, we replaced the
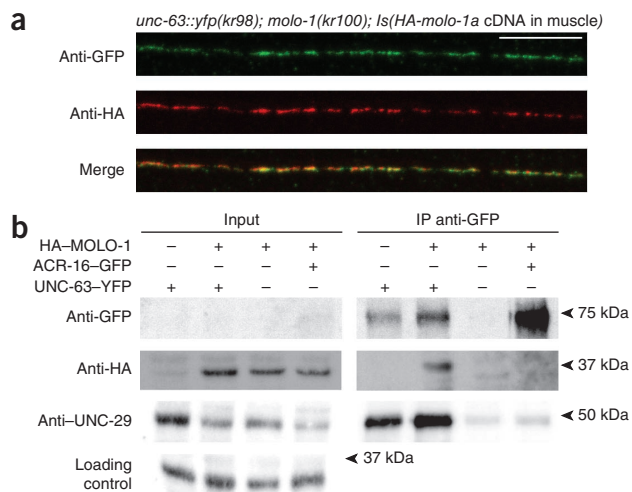
TPM domain with that of the closely related R02D5.3 protein. This protein was not targeted to synapses, and we observed no phenotypic rescue. Therefore, both trafficking and function of MOLO-1 are dependent on its extracellular TPM and transmembrane domains, whereas its intracellular C terminus is dispensable for protein localization and function.

MOLO-1 and L-AChRs form a receptor complex *in vivo*

After establishing, on the basis of genetic and electrophysiological evidence, that MOLO-1 and L-AChRs functionally interacted, we tested whether they formed a biochemical complex *in vivo*. First, we generated a stable transgenic line expressing a hemagglutinin (*HA*)-tagged *molo-1a* cDNA in body wall muscle. This transgene restored wild-type levamisole sensitivity in *molo-1* mutants (**Fig. 3g**), and the HA–MOLO-1 fusion protein was localized to L-AChR–containing synapses (**Fig. 4a**). Next, we combined this transgene with the *unc-63::yfp(kr98)* knock-in strain and with a muscle-expressed *acr-16::gfp(jaSi4)* single-copy integrant[30].

Using antibodies that recognize GFP and YFP, we were able to immunoprecipitate UNC-63–YFP and ACR-16–GFP from total membrane preparations (**Fig. 4b**). We then observed that HA–MOLO-1A coimmunoprecipitated with UNC-63–YFP L-AChR but not with ACR-16–GFP N-AChR, establishing that MOLO-1 and L-AChRs specifically interacted in a physical complex (**Fig. 4b** and **Supplementary Fig. 4b**).

MOLO-1 binds to L-AChRs early in the secretory pathway

Although we demonstrated that MOLO-1 and L-AChR could be coimmunoprecipitated *in vivo*, this did not formally exclude the possibility of an indirect interaction. We therefore attempted to demonstrate a direct interaction between MOLO-1 with L-AChRs by performing coimmunoprecipitation experiments in a heterologous expression system. L-AChRs and N-AChRs can be functionally reconstituted
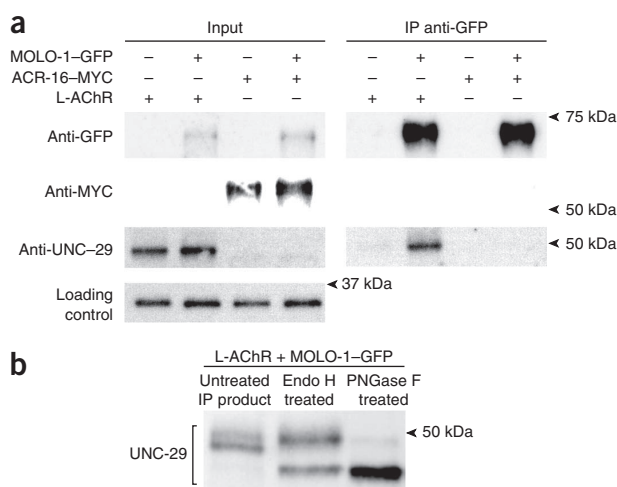

Figure 5 MOLO-1 binds directly to L-AChRs early in the secretory pathway. (**a**) L-AChRs, but not N-AChRs, immunoprecipitate with MOLO-1 in *Xenopus* oocytes. Immunoprecipitation of MOLO-1–GFP with anti-GFP was followed by western blot analysis using anti–UNC-29 for L-AChRs and anti-myc for myc-tagged N-AChRs (ACR-16–myc). MOLO-1–GFP is visualized using anti-GFP. A nonspecific band labeled by anti-UNC-29 in all samples was used as a loading control. (**b**) UNC-29 proteins that immunoprecipitated with MOLO-1–GFP have a larger apparent molecular weight than UNC-29 in *C. elegans* extracts. Endo H treatment converts higher to lower molecular weight forms. PNGase F treatment removes all glycosylation, resulting in UNC-29 proteins of the expected molecular weight.

Figure 6 MOLO-1 increases L-AChR gating.
(**a**) Expression of MOLO-1 with L-AChRs in *Xenopus* oocytes increased mean peak currents 1.94-, 1.78- and 1.86-fold in three independent experiments. For N-AChR, average currents were not significantly increased. Mean ± s.e.m., *n* = number of cells, Student's *t*-test; *$P < 0.05$, **$P < 0.005$; NS, not significant. (**b**) Single-channel conductance. Chord conductance at −80 mV: 30.8 ± 2.1 pS (*n* = 5) for L-AChR versus 31.8 ± 1.8 pS (*n* = 8) for L-AChR + MOLO-1, Student's *t*-test, $P = 0.38$. Channel openings were elicited by application of 10 μM acetylcholine (ACh) in outside-out patches. Representative single-channel openings, bottom left; corresponding amplitude histograms, bottom right. (**c**) MOLO-1 increases the apparent affinity of L-AChR for levamisole. At −60 mV holding potential, ACh EC$_{50}$ values were 24.2 ± 0.65 μM (Hill coefficient $n_H = 1.02 ± 0.02$; *n* = 5) and 22.4 ± 0.7 μM ($n_H = 1.00 ± 0.03$; *n* = 6) for L-AChR and L-AChR + MOLO-1, respectively; levamisole EC$_{50}$ values, 17.1 ± 2.7 μM ($n_H = 0.92 ± 0.07$;

n = 5) and 9.7 ± 1.0 μM ($n_H = 1.03 ± 0.07$; *n* = 5) for L-AChR and L-AChR + MOLO-1, respectively. The values for 500 μM levamisole were excluded from the fit because of open channel block at this concentration. Mean ± s.d. (**d**) Sensitivity to the pore blocker QX-314. At a holding potential of −60 mV, the IC$_{50}$ of QX-314 was 28.2 ± 2.4 μM ($n_H = 1.02 ± 0.08$; *n* = 5) and 9.6 ± 0.5 μM ($n_H = 0.94 ± 0.04$; *n* = 5) for L-AChR and L-AChR + MOLO-1, respectively. Mean ± s.d. Inset: overlayed current traces ([ACh], 100 μM; [QX-314], 30 μM; holding potential, −60 mV). (**e**) Voltage dependence of QX-314 block in the presence and absence of MOLO-1. Slope (voltage dependence) of the linear fit: *e*-fold change per 30 mV and 26 mV without and with MOLO-1, respectively. IC$_{50}$ values were deduced from full dose-response curves established at −20, −40, −60 and −80 mV in the presence of 100 μM ACh (see **Supplementary Fig. 8**). Mean ± s.d.
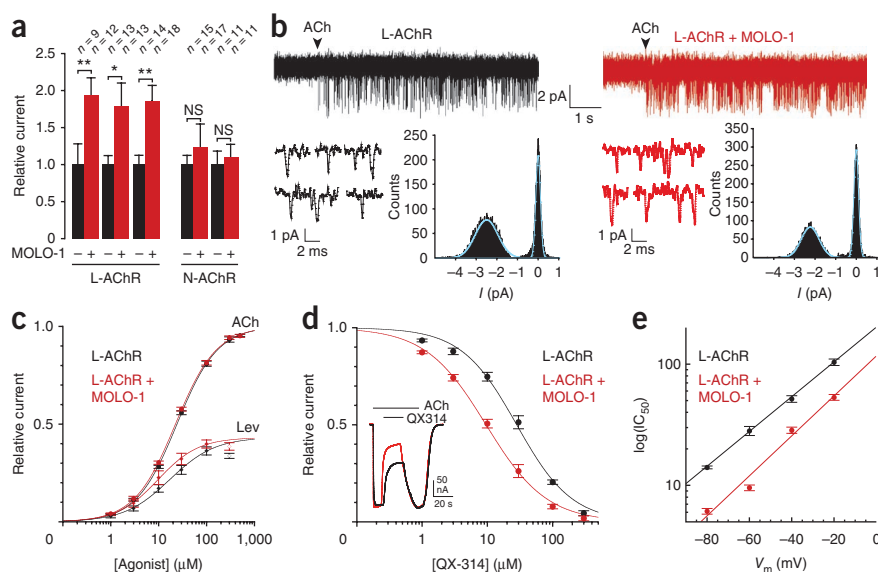
in *Xenopus* oocytes[13]. As there are no immunoprecipitating antibodies for L-AChR or N-AChR subunits, we coexpressed L-AChRs or myc-tagged N-AChRs (ACR-16–myc) with a full-length MOLO-1–GFP fusion as a substrate for immunoprecipitation. UNC-29 L-AChR and ACR-16–myc subunits were readily detected in solubilized membrane preparations from oocytes expressing functional receptors (**Fig. 5a** and **Supplementary Fig. 4c**). Using antibodies to GFP, we immunoprecipitated the L-AChR subunit UNC-29 but not ACR-16–myc with MOLO-1–GFP, demonstrating that MOLO-1 and L-AChRs interact physically and specifically.

Of note, the apparent size of the UNC-29 subunit was consistently larger in *Xenopus* oocyte extracts than in *C. elegans* extracts. This could be explained by increased glycosylation of UNC-29 in oocytes. We took advantage of this feature to test whether MOLO-1 interacted with L-AChRs early in the secretory pathway, as suggested by MOLO-1's dependence on L-AChRs for trafficking to the cell surface *in vivo*. We coimmunoprecipitated UNC-29 subunits with MOLO-1–GFP and treated them either with Endo H, which cleaves simple N-glycans present on proteins from the endoplasmic reticulum or early Golgi apparatus, or with PNGase F, which removes all N-glycan moieties. Both treatments converted UNC-29 proteins from higher to lower molecular weights (**Fig. 5b**), but the partial effect of Endo H suggested that some of the L-AChRs that immunoprecipitated with MOLO-1–GFP originated from endoplasmic reticulum or Golgi membranes. These data demonstrate that MOLO-1 interacts with L-AChRs at early stages of the secretory pathway, confirming the *in vivo* data above.

MOLO-1 increases L-AChR gating

To further investigate the mechanism of action of MOLO-1, we analyzed its functional effects on L-AChRs expressed in *Xenopus* oocytes. As expected from our *in vivo* data, we observed an approximately twofold increase in the maximum amplitude of acetylcholine-induced currents when MOLO-1 was coexpressed with L-AChRs (**Fig. 6a**).

This was not the case when MOLO-1 was coexpressed with N-AChR (**Fig. 6a**) or when the MOLO-1 paralog R02D5.3 was expressed with L-AChR (**Supplementary Fig. 7a**), underscoring the specificity for L-AChRs of MOLO-1 modulation. As MOLO-1 does not affect the expression or trafficking of L-AChRs, this increase in current amplitude could be explained by an increase in the channel's unitary conductance or by an increase in its open probability. To examine these two possibilities, we recorded single-channel activity of L-AChRs in the presence or absence of MOLO-1 in excised outside-out patches from *Xenopus* oocytes. Application of acetylcholine triggered single-channel responses in both conditions, and analysis of amplitude distributions revealed that expression of MOLO-1 did not significantly modify the channel's unitary conductance (**Fig. 6b**). Observed values were consistent with data obtained from *C. elegans* primary cell cultures[31] and adult muscle patches[32]. Therefore, this result suggested that MOLO-1 likely modifies the channel's open probability.

The excessively short durations of channel openings (<500 μs) precluded us from accurately extracting open-probability values from single-channel traces. Therefore, to assess possible changes in open probability, we turned to an approach relying on macroscopic current measurements. Because changes in channel open probability may translate into changes in agonist sensitivity[33], we first generated full dose-response curves for the agonists acetylcholine and levamisole. Whereas the sensitivity for acetylcholine was not markedly modified by the addition of MOLO-1, the levamisole sensitivity was modestly but significantly increased (Student *t*-test, $P < 0.05$ for all concentrations except at 1 μM at the very foot of the curves), compatible with an enhanced channel open probability in the presence of MOLO-1 (**Fig. 6c**). We next compared the sensitivity of L-AChRs to open channel blockers, whose potency should increase (that is, IC$_{50}$ should decrease) with increasing channel open probability[34]. MOLO-1 coexpression resulted in a marked and consistent increase in L-AChR sensitivity to the blockers QX-314, QX-222 and mecamylamine (**Fig. 6d, Supplementary Fig. 8**

and **Supplementary Table 2**), supporting an increased channel activity. In contrast, we observed no effect when coexpressing the MOLO-1 paralog R02D5.3 (**Supplementary Fig. 7b**). We further investigated the mechanism of action of MOLO-1 by measuring the IC_{50} of QX-314 in the presence or absence of MOLO-1 at various holding potentials. MOLO-1 enhanced the sensitivity of L-AChR to QX-314 at all potentials tested. Most importantly, MOLO-1 produced a marked rightward shift of the relation describing the voltage dependence of QX-314 affinity but had little effect on the slope of the curve (**Fig. 6e**). These data are a strong indication that the main effect of MOLO-1 is to change the apparent affinity of the pore-blocking site for QX-314 without changing the effective location (that is, the electrical depth) of the blocking site within the ion channel, as expected from an allosteric mechanism of action. This observation further strengthens our hypothesis that MOLO-1 modifies L-AChR gating, most likely by interacting directly with the receptor and promoting channel opening.

DISCUSSION

The data presented here show that MOLO-1 fulfils all the criteria of an auxiliary subunit for the levamisole-sensitive AChR: first, MOLO-1 is a transmembrane protein that does not contribute to the pore of the channel, on the basis of the evolutionary conservation of AChR structure and the absence of an effect on channel conductance; second, it directly and stably interacts with the pore-forming subunits early in the secretory pathway and requires the receptor for trafficking to the plasma membrane; third, MOLO-1 modifies the activity of the L-AChR, acting as a positive allosteric modulator; fourth, it is required for the function of the receptor *in vivo*, as its removal causes locomotory defects and resistance to levamisole.

Conservation of TPM domain–containing proteins

The extracellular region of MOLO-1 contains a single TPM domain. Our bioinformatic analysis revealed that the TPM domain is an ancient protein fold conserved in bacteria, plants, protozoa and metazoa. The primary sequences of TPM domain–containing proteins have diverged greatly; nevertheless available structural data reveal a well-conserved tertiary structure. Although TPM-containing proteins are present in several taxa of both protostomes and deuterostomes, they are not found in the genomes of vertebrates. This absence is surprising because the genome of the lancelet *Branchiostoma floridae*, the closest nonvertebrate chordate, contains seven genes encoding TPM-containing proteins. We speculate that TPM domains may either have been lost in the vertebrate lineage or undergone major rearrangements making them impossible to detect using available search tools.

As yet, the only characterized TPM-containing proteins are the *Arabidopsis thaliana* protein AtTLP18.3 (ref. 35) and *Synechocystis* sp. PCC 6803 protein Psb32 (refs. 36,37). Both are transmembrane auxiliary subunits associated with photosystem II (PSII). They are involved in PSII dimerization and removal of damaged D1 proteins[35,37]. AtTLP18.3 was recently suggested to possess an acid phosphatase activity[27]. It is unlikely that MOLO-1 serves a similar function in *C. elegans*, as the TPM domain of MOLO-1 is located in the extracellular space, whereas kinases and phosphatases function intracellularly. Furthermore, two of the residues of AtTLP18.3 that contribute to phospho-substrate binding are not conserved in metazoa. We therefore conclude that the TPM domain has been conserved structurally but recruited for new functions during evolution.

MOLO-1 helps define the composition of endogenous L-AChRs

Inactivation of *molo-1* in *C. elegans* causes two main phenotypes: mild but consistent defects in locomotion and decreased sensitivity to levamisole. Reconstitution of *Haemonchus contortus* and *Ascaris suum* L-AChRs has revealed notable differences from the *C. elegans* receptor in pharmacology[38,39]. On the basis of our data and the strong sequence conservation, L-AChRs from parasitic nematodes most likely contain MOLO-1 orthologs. As L-AChRs are important drug targets for the treatment of parasitic nematode infections, it will be important to include MOLO-1 in future L-AChR reconstitutions when screening for new anthelmintic drugs.

Analysis of *molo-1* paralogs might also be relevant for anti-parasitic treatments, as other nematode Cys-loop receptors are targeted by anthelmintic drugs, including the amino acetonitrile derivatives (AADs) such as monepantel, which target ionotropic AChRs[40], and ivermectin, which activates glutamate-gated chloride channels in nematodes[41]. Given the strong structural similarities between glutamate-gated chloride channels and AChRs[42], it is possible that paralogs of MOLO-1 could act as auxiliary subunits for these receptors and therefore represent plausible candidates for drug-resistance loci.

Regulation of Cys-loop receptor function

Previously, only prototoxins had been shown to modulate AChR function[43]. These are small extracellular proteins similar to α-bungarotoxin that are either secreted[44] (SLURP peptides) or glycosyl phosphatidylinositol (GPI)–anchored[45] (Lynx proteins). Several prototoxins interact with the acetylcholine-binding sites of certain AChR isotypes[46] and produce negative and positive allosteric modulation when applied as soluble peptides to heterologously expressed AChRs, therefore defining them as endogenous regulators rather than bona fide auxiliary subunits[43,47].

Why do L-AChRs need an auxiliary subunit at *C. elegans* neuromuscular junctions? MOLO-1 clearly is important physiologically. Loss of *molo-1* results in significant locomotory impairment, which could be detrimental to survival of animals in the wild. Consistently, high levels of sequence conservation between MOLO-1 orthologs in distant nematode species suggests that this function may have been conserved during nematode evolution. As acetylcholine is the main excitatory neurotransmitter in the *C. elegans* nervous system, the use of auxiliary proteins might represent a means to increase the functional repertoire of ionotropic acetylcholine receptors. One hypothesis would be that regulation of MOLO-1 expression could serve as a regulatory switch to attenuate or augment L-AChR function without modifying receptor expression itself.

MOLO-1 is, to our knowledge, the first example of a bona fide auxiliary subunit for a ligand-gated ion channel of the Cys-loop receptor family. To what extent is this finding relevant for vertebrate AChRs and other members of the Cys-loop receptor family? The first auxiliary subunit of glutamate receptors, stargazin, was identified many years after the cloning of AMPA receptor subunits, by analyzing the stargazer mouse mutant, which lacked AMPA receptors at specific synapses in the cerebellum[48]. This discovery stimulated the search for additional accessory subunits. Remarkably, genetic and biochemical strategies identified diverse and structurally unrelated proteins such as TARPs, cornichon homologs, and NETO1 and NETO2 (refs. 1,3,5,7). The possibility that proteins structurally different from MOLO-1 could associate with AChRs or other Cys-loop receptors therefore appears plausible. In addition, the presence of auxiliary subunits in native receptors is not always easy to anticipate. In some cases, functional discrepancies between native and reconstituted receptors predicted the existence of auxiliary subunits[5,7]. In contrast, identification of MOLO-1 originated from the characterization of a mutant strain with decreased sensitivity to levamisole, whereas the properties of native and reconstituted L-AChRs were not obviously different at first glance. Therefore, even

when recombinant and native receptors have similar properties, auxiliary subunits may act in the physiological regulation of these channels. Identification of MOLO-1 demonstrates that Cys-loop receptors are amenable to regulation by auxiliary subunits, a concept that might be extended to other Cys-loop receptors in mammals.

METHODS

Methods and any associated references are available in the online version of the paper.

Note: Supplementary information is available in the online version of the paper.

AUTHOR CONTRIBUTIONS
T.B., G.R., L.B.-R., C.S., P.P. and J.-L.B. conceived the ideas and designed the experiments. T.B., G.R., L.B.-R., C.S. and J.E.R. performed the experiments. T.B., G.R., L.B.-R., C.S., J.E.R. and P.P. analyzed the data. T.B., P.P. and J.-L.B. wrote the paper.

COMPETING FINANCIAL INTERESTS
The authors declare no competing financial interests.

1. Tomita, S. *et al.* Functional studies and distribution define a family of transmembrane AMPA receptor regulatory proteins. *J. Cell Biol.* **161**, 805–816 (2003).
2. von Engelhardt, J. *et al.* CKAMP44: a brain-specific protein attenuating short-term synaptic plasticity in the dentate gyrus. *Science* **327**, 1518–1522 (2010).
3. Schwenk, J. *et al.* Functional proteomics identify cornichon proteins as auxiliary subunits of AMPA receptors. *Science* **323**, 1313–1319 (2009).
4. Walker, C.S. *et al.* Conserved SOL-1 proteins regulate ionotropic glutamate receptor desensitization. *Proc. Natl. Acad. Sci. USA* **103**, 10787–10792 (2006).
5. Zhang, W. *et al.* A transmembrane accessory subunit that modulates kainate-type glutamate receptors. *Neuron* **61**, 385–396 (2009).
6. Kato, A.S. *et al.* Hippocampal AMPA receptor gating controlled by both TARP and cornichon proteins. *Neuron* **68**, 1082–1096 (2010).
7. Straub, C. *et al.* Distinct functions of kainate receptors in the brain are determined by the auxiliary subunit Neto1. *Nat. Neurosci.* **14**, 866–873 (2011).
8. Jackson, A.C. & Nicoll, R.A. The expanding social network of ionotropic glutamate receptors: TARPs and other transmembrane auxiliary subunits. *Neuron* **70**, 178–199 (2011).
9. Sumioka, A. *et al.* PDZ binding of TARPγ-8 controls synaptic transmission but not synaptic plasticity. *Nat. Neurosci.* **14**, 1410–1412 (2011).
10. Richmond, J.E. & Jorgensen, E.M. One GABA and two acetylcholine receptors function at the *C. elegans* neuromuscular junction. *Nat. Neurosci.* **2**, 791–797 (1999).
11. Ballivet, M., Alliod, C., Bertrand, S. & Bertrand, D. Nicotinic acetylcholine receptors in the nematode *Caenorhabditis elegans. J. Mol. Biol.* **258**, 261–269 (1996).
12. Touroutine, D. *et al. acr-16* encodes an essential subunit of the levamisole-resistant nicotinic receptor at the *Caenorhabditis elegans* neuromuscular junction. *J. Biol. Chem.* **280**, 27013–27021 (2005).
13. Boulin, T. *et al.* Eight genes are required for functional reconstitution of the *Caenorhabditis elegans* levamisole-sensitive acetylcholine receptor. *Proc. Natl. Acad. Sci. USA* **105**, 18590–18595 (2008).
14. Fleming, J.T. *et al. Caenorhabditis elegans* levamisole resistance genes *lev-1, unc-29,* and *unc-38* encode functional nicotinic acetylcholine receptor subunits. *J. Neurosci.* **17**, 5843–5857 (1997).
15. Lewis, J.A., Wu, C.H., Berg, H. & Levine, J.H. The genetics of levamisole resistance in the nematode *Caenorhabditis elegans. Genetics* **95**, 905–928 (1980).
16. Culetto, E. *et al.* The *Caenorhabditis elegans unc-63* gene encodes a levamisole-sensitive nicotinic acetylcholine receptor α subunit. *J. Biol. Chem.* **279**, 42476–42483 (2004).
17. Towers, P.R., Edwards, B., Richmond, J.E. & Sattelle, D.B. The *Caenorhabditis elegans lev-8* gene encodes a novel type of nicotinic acetylcholine receptor alpha subunit. *J. Neurochem.* **93**, 1–9 (2005).
18. Eimer, S. *et al.* Regulation of nicotinic receptor trafficking by the transmembrane Golgi protein UNC-50. *EMBO J.* **26**, 4313–4323 (2007).
19. Halevi, S. *et al.* The *C. elegans ric-3* gene is required for maturation of nicotinic acetylcholine receptors. *EMBO J.* **21**, 1012–1020 (2002).
20. Gally, C., Eimer, S., Richmond, J.E. & Bessereau, J.L. A transmembrane protein required for acetylcholine receptor clustering in *Caenorhabditis elegans. Nature* **431**, 578–582 (2004).
21. Gendrel, M., Rapti, G., Richmond, J.E. & Bessereau, J.L. A secreted complement-control-related protein ensures acetylcholine receptor clustering. *Nature* **461**, 992–996 (2009).
22. Rapti, G., Richmond, J. & Bessereau, J.L. A single immunoglobulin-domain protein required for clustering acetylcholine receptors in *C. elegans. EMBO J.* **30**, 706–718 (2011).
23. Bessereau, J.L. *et al.* Mobilization of a *Drosophila* transposon in the *Caenorhabditis elegans* germ line. *Nature* **413**, 70–74 (2001).
24. Boulin, T. & Bessereau, J.L. Mos1-mediated insertional mutagenesis in *Caenorhabditis elegans. Nat. Protoc.* **2**, 1276–1287 (2007).
25. Williams, D.C., Boulin, T., Ruaud, A.F., Jorgensen, E.M. & Bessereau, J.L. Characterization of Mos1-mediated mutagenesis in *Caenorhabditis elegans*: a method for the rapid identification of mutated genes. *Genetics* **169**, 1779–1785 (2005).
26. Eletsky, A. *et al.* Solution NMR structures reveal a distinct architecture and provide first structures for protein domain family PF04536. *J. Struct. Funct. Genomics* **13**, 9–14 (2012).
27. Wu, H.Y., Liu, M.S., Lin, T.P. & Cheng, Y.S. Structural and functional assays of AtTLP18.3 identify its novel acid phosphatase activity in thylakoid lumen. *Plant Physiol.* **157**, 1015–1025 (2011).
28. Robert, V. & Bessereau, J.L. Targeted engineering of the *Caenorhabditis elegans* genome following Mos1-triggered chromosomal breaks. *EMBO J.* **26**, 170–183 (2007).
29. Gottschalk, A. & Schafer, W.R. Visualization of integral and peripheral cell surface proteins in live *Caenorhabditis elegans. J. Neurosci. Methods* **154**, 68–79 (2006).
30. Sancar, F. *et al.* The dystrophin-associated protein complex maintains muscle excitability by regulating Ca^{2+}-dependent K^+ (BK) channel localization. *J. Biol. Chem.* **286**, 33501–33510 (2011).
31. Rayes, D., Flamini, M., Hernando, G. & Bouzat, C. Activation of single nicotinic receptor channels from *Caenorhabditis elegans* muscle. *Mol. Pharmacol.* **71**, 1407–1415 (2007).
32. Qian, H., Robertson, A.P., Powell-Coffman, J.A. & Martin, R.J. Levamisole resistance resolved at the single-channel level in *Caenorhabditis elegans. FASEB J.* **22**, 3247–3254 (2008).
33. Colquhoun, D. Binding, gating, affinity and efficacy: the interpretation of structure-activity relationships of agonists and of the effects of mutating receptors. *Br. J. Pharmacol.* **125**, 924–947 (1998).
34. Neher, E. & Steinbach, J.H. Local anaesthetics transiently block currents through single acetylcholine-receptor channels. *J. Physiol. (Lond.)* **277**, 153–176 (1978).
35. Sirpiö, S. *et al.* TLP18.3, a novel thylakoid lumen protein regulating photosystem II repair cycle. *Biochem. J.* **406**, 415–425 (2007).
36. Kashino, Y. *et al.* Proteomic analysis of a highly active photosystem II preparation from the cyanobacterium *Synechocystis* sp. PCC 6803 reveals the presence of novel polypeptides. *Biochemistry* **41**, 8004–8012 (2002).
37. Wegener, K.M., Bennewitz, S., Oelmuller, R. & Pakrasi, H.B. The Psb32 protein aids in repairing photodamaged photosystem II in the cyanobacterium *Synechocystis* 6803. *Mol. Plant* **4**, 1052–1061 (2011).
38. Boulin, T. *et al.* Functional reconstitution of *Haemonchus contortus* acetylcholine receptors in *Xenopus* oocytes provides mechanistic insights into levamisole resistance. *Br. J. Pharmacol.* **164**, 1421–1432 (2011).
39. Williamson, S.M. *et al.* The nicotinic acetylcholine receptors of the parasitic nematode *Ascaris suum*: formation of two distinct drug targets by varying the relative expression levels of two subunits. *PLoS Pathog.* **5**, e1000517 (2009).
40. Kaminsky, R. *et al.* A new class of anthelmintics effective against drug-resistant nematodes. *Nature* **452**, 176–180 (2008).
41. Dent, J.A., Smith, M.M., Vassilatis, D.K. & Avery, L. The genetics of ivermectin resistance in *Caenorhabditis elegans. Proc. Natl. Acad. Sci. USA* **97**, 2674–2679 (2000).
42. Hibbs, R.E. & Gouaux, E. Principles of activation and permeation in an anion-selective Cys-loop receptor. *Nature* **474**, 54–60 (2011).
43. Miwa, J.M., Freedman, R. & Lester, H.A. Neural systems governed by nicotinic acetylcholine receptors: emerging hypotheses. *Neuron* **70**, 20–33 (2011).
44. Chimienti, F. *et al.* Identification of SLURP-1 as an epidermal neuromodulator explains the clinical phenotype of Mal de Meleda. *Hum. Mol. Genet.* **12**, 3017–3024 (2003).
45. Miwa, J.M. *et al.* lynx1, an endogenous toxin-like modulator of nicotinic acetylcholine receptors in the mammalian CNS. *Neuron* **23**, 105–114 (1999).
46. Lyukmanova, E.N. *et al.* NMR structure and action on nicotinic acetylcholine receptors of water-soluble domain of human LYNX1. *J. Biol. Chem.* **286**, 10618–10627 (2011).
47. Morishita, H., Miwa, J.M., Heintz, N. & Hensch, T.K. Lynx1, a cholinergic brake, limits plasticity in adult visual cortex. *Science* **330**, 1238–1240 (2010).
48. Letts, V.A. *et al.* The mouse stargazer gene encodes a neuronal Ca^{2+}-channel γ subunit. *Nat. Genet.* **19**, 340–347 (1998).

ONLINE METHODS

General methods. Strains were maintained at 20 °C on NGM agar plates. *Mos1* mutagenesis was performed according to published protocols[24]. For levamisole resistance assays, young adult worms were transferred to 0.6 mM levamisole plates and scored after 12 to 18 h at 20 °C. For thrashing assays, young adult worms were placed in M9 at 20 °C and videotaped for 5 min. Thrashes were counted in 30-s intervals after the first minute.

Germline transformation. Germline transformation was achieved by microinjecting DNA mixes into the gonads of adult hermaphrodites.

For *molo-1(kr100)* rescue, animals were injected with a DNA mixture containing the F09F7.1 genomic fragment (5 ng·μL⁻¹), pHU4 (*Prab-3::gfp*, 20 ng·μL⁻¹), pPD115.62 (*Pmyo-3::gfp*, 5 ng·μL⁻¹) and 1-kb ladder (Invitrogen, 70 ng·μL⁻¹).

For expression pattern analysis, pTB198 (*Pmolo-1::molo-1-SL2-gfp*, 10 ng·μL⁻¹) was injected with pPD97/98 (*Punc-122::gfp*, 20 ng·μL⁻¹) and 1-kb ladder (70 ng·μL⁻¹) into *molo-1(kr100)*.

For tissue-specific rescue, pTB195 (*Pmyo-3::molo-1a*, 5 ng·μL⁻¹), pTB287 (*Pmyo-3::molo-1b*, 5 ng·μL⁻¹) or pTB196 (*Prab-3::molo-1a*, 5 ng·μL⁻¹) were injected with pPD97/98 (*Punc-122::gfp*, 20 ng·μL⁻¹) and 1-kb ladder (100 ng·μL⁻¹) into *molo-1(kr100)*.

For subcellular localization, pTB201 (*Pmyo-3::gfp-molo-1a*, 2.5 ng·μL⁻¹), pTB233 (*Pmyo-3::gfp-molo-1{intra}*, 2.5 ng·μL⁻¹), pTB261 (*Pmyo-3::gfp-molo-1{TM-intra}-CD4*, 2.5 ng·μL⁻¹), pTB268 (*Pmyo-3::gfp-R02D5.3{TPM}-molo-1a{TM-intra}*, 2.5 ng·μL⁻¹) and pTB229 (*Pmyo-3::HA-molo-1a*, 2.5 ng·μL⁻¹) were each injected with pPD97/98 (*Punc-122::gfp*, 20 ng·μL⁻¹) and 1-kb ladder (100 ng·μL⁻¹) into *molo-1(kr100)*. pTB222 (*Pmyo-3::molo-1{TM-intra}-gfp*, 2.5 ng·μL⁻¹) was injected with pPD118.33 (*Pmyo-2::gfp*, 20 ng·μL⁻¹) and 1-kb ladder (100 ng·μL⁻¹) into *molo-1(kr100)*. The transgenic line resulting from the injection of pTB229 (*Pmyo-3::HA-molo-1a*) was later integrated into the genome by gamma ray irradiation, resulting in the stable line *krIs45*.

For the *Mos*TIC experiment resulting in the *unc-29::myc(kr244)* knock-in strain, CSp013 (*unc-29::myc* repair template, 50 ng·μL⁻¹) was injected with pPD118.33 (*Pmyo-2::gfp*, 23 ng·μL⁻¹) and pJL44 (*Phsp-16.48::transposase*, 50 ng·μL⁻¹) into *unc-29(kr158); acr-16(ok789)*.

Immunohistochemical staining. Worms were prepared for immunohistochemistry following previously published protocols[21]. In brief, worms were washed in ice-cold water, freeze-cracked and fixed in −20 °C methanol and −20 °C acetone for 5 min each. Samples were blocked for 30 min at room temperature with 0.2% fish gelatin. Primary antibodies were used at the following dilutions: anti-UNC-38 (ref. 21), 1:800; anti-UNC-17 (ref. 20), 1:3,000; polyclonal rabbit anti-GFP (Molecular Probes A11122, Invitrogen), 1:500; monoclonal mouse anti-GFP (Roche 1814460), 1:500. Secondary antibodies included Cy3-labeled goat anti-rabbit IgG (H+L) used at 1:1,000 (Jackson ImmunoResearch Laboratories A10520, Invitrogen), Cy3-labeled goat anti-mouse IgG (H+L) at 1:1,000 (Jackson ImmunoResearch Laboratories A10521, Invitrogen), Alexa 488–labeled goat anti-rabbit IgG (H+L) (Molecular Probes A-11008, Invitrogen) at 1:500 and Alexa 488–labeled goat anti-mouse IgG at 1:500 (Molecular Probes A-11001, Invitrogen).

Electrophysiology. *C. elegans electrophysiology.* Electrophysiological responses were recorded using previously described procedures[10]. In brief, worms were immobilized with cyanoacrylate glue and cut open to expose neuromuscular junctions, and muscles were whole-cell voltage-clamped at a holding potential of −60 mV.

Two-electrode voltage-clamp in Xenopus oocytes. Electrophysiological recordings were performed as previously described[13].

For agonist dose-response curves, data points were obtained from BAPTA-AM-treated oocytes and fitted with the following Hill equation: $I_{rel} = I_{max}/(1+(EC_{50}/[A])^{n_H})$, where I_{rel} is the mean relative current, I_{max} is the relative current obtained at saturating concentrations of agonist, [A] is the agonist concentration, n_H is the Hill coefficient and EC_{50} is the concentration of agonist producing 50% of the maximal current. EC_{50}, I_{max} and n_H were fitted as free parameters. For ACh, data points were divided by the fitted I_{max} value to obtain normalized currents. Resulting values for each individual cell and for each agonist concentration were then averaged, and the mean data points were fitted with the same Hill equation as above but with I_{max} fixed to 1.

For levamisole dose-response curves, only one data point was collected per oocyte and was normalized to the current evoked by 500 μM ACh. For antagonist dose-response curves, inhibition was measured relative to the current evoked by 100 μM ACh and the resulting data were fitted with the following Hill equation: $I_{rel} = 1 - 1/(1+(IC_{50}/[Ant])^{n_H})$, where I_{rel} is the mean relative current, I_{max} is the relative current obtained at saturating concentrations of agonist, [Ant] is the antagonist concentration, n_H is the Hill coefficient and IC_{50} is the concentration of antagonist producing 50% of the maximal inhibition. IC_{50} and n_H were fitted as free parameters. The dependence of QX-314's apparent affinity (IC_{50}) to membrane voltage (V_m) was analyzed using a simple one-site voltage-dependent channel block mechanism[49] and assuming no permeation of QX-314 through the channel. In such a mechanism, the relationship between IC_{50} and V_m obeys the following equation: $IC_{50} = IC_{50_{0mV}} \times e^{z\delta FV/RT}$, with z being the valence of QX-314 (+1) and δ the apparent electrical distance from the extracellular medium to the blocker binding site (the 'electrical depth').

Single-channel recordings. Vitelline membranes were removed manually from oocytes immediately before patching. Recordings were performed on outside-out patches using patch pipettes of 4–5 MΩ that were filled with an internal solution containing (in mM): 10 HEPES pH = 7.24, 115 CsF, 10 CsCl, 10 BAPTA free acid. The final osmolality was 270 mosmol·kg⁻¹. The external recording solution was (in mM): 10 HEPES pH = 7.2, 140 NaCl, 2.8 KCl, 1 CaCl₂. Experiments were performed at room temperature using an Axopatch 200B amplifier. Currents were sampled at 100 kHz and filtered at 2–5 kHz. Amplitude histograms were constructed from idealized traces using the event detection protocol with a 50% threshold criteria and excluding events shorter than 0.2 ms.

MosTIC experiment and antibody injection. Creation of *unc-29::myc*. Starting from an almost paralyzed *unc-29(kr158); acr-16(ok789)* double mutant (*Mos1* insertion 667 bp from the *unc-29* 3′ end), we generated transgenic lines by coinjecting the heat-shock inducible *Mos1* transposase transgene (pJL44) and an *in vitro*–engineered repair template (CSp013) (**Supplementary Fig. 5**). This repair template contains a portion of the genomic region of *unc-29* modified at the 3′ end by the insertion of three myc tag sequences. This repair template alone does not rescue the *unc-29* mutant, and therefore only *Mos*TIC events in which the endogenous locus is repaired by homologous recombination will restore wild-type locomotion to these mutant worms.

Antibody injection. Anti-GFP–Alexa 594 (Molecular Probes A-21312) and anti-c-myc–Cy3 (Sigma C6594) were diluted 200-fold in injection buffer (20 mM K₂HPO₄, 3 mM K⁺ citrate, 2% PEG 6000, pH = 7.5) and injected into the pseudocoelomic cavity using an injection setup designed for germline transformation[29]. Worms were imaged 4 to 6 h after injection. Fluorescence was readily visible in coelomocytes, which take up unbound fluorescent antibodies from the extracellular milieu.

Quantification of synaptic fluorescence. *Quantification of unc-63::yfp fluorescence.* *unc-63::yfp(kr98)*-containing strains were mounted on agarose pads and immobilized with sodium azide for confocal imaging. Image stacks of the anterior portion of the dorsal nerve cord were acquired and analyzed by summing the total fluorescence in a manually defined region of interest (ROI). This fluorescence intensity was then normalized by the length of the chosen ROI. Background fluorescence was very similar between samples.

Quantification of anti-myc–Cy3 fluorescence. A *z*-stack of approximately 10 μm of the anterior portion of the dorsal nerve cord of *unc-29::myc(kr244)* worms injected with anti-c-myc–Cy3) were acquired and projected into a single plane image. A gaussian vertical profile was obtained from the most anterior 10 μm of the cord using ImageJ (NIH, USA). A background line was defined using the 'tail' values, and at each point of the curve the corresponding background value was subtracted. The total intensity was obtained by summing the resulting adjusted values. The macros used for the quantification are available upon request.

Homology modeling. Homology models for the TPM domain of MOLO-1 were calculated with Accelrys Discovery Studio 2.5 using the 2KW7 and 2KPT PDB entries as templates. Primary sequence alignments were generated with t-coffee (EBI) and optimized manually before simulation. The models with the lowest free

energy values generated with either template had very similar overall structures. All renderings were created with PyMOL (http://www.pymol.org/).

Biochemistry. *Immunoprecipitation using* Xenopus *oocyte extracts.* Four to five days before homogenization, *Xenopus laevis* oocytes were prepared and injected as described previously[13]. On the day of the experiment, oocytes were screened for receptor expression by two-electrode voltage clamp. Oocyte membrane extractions were prepared as previously described with the following modifications[50]. Twelve oocytes with currents ranging from 1 to 10 µA were pooled and suspended in 1 mL ice-cold oocyte homogenization buffer 1 (OHB1: 50 mM HEPES pH = 7.5, 150 mM NaCl, 1 mM PMSF, 1 mM EDTA pH = 8.0 and Complete Protease Inhibitor, Roche). Oocytes were homogenized and cleared supernatants were obtained by two consecutive centrifugations at 2,000g for 10 min at 4 °C. Membrane preparations were obtained by ultracentrifugation at 50,000g for 30 min at 4 °C. Pellets were resuspended and incubated for 30 min in 0.1 mL ice-cold OHB1 including 1% (w/v) Triton X-100. The mix was further diluted to 0.5 mL with ice-cold OHB1 (final concentration of 0.2% (w/v) Triton X-100) and sonicated in a Leo L-801 ultrasonic cleaner for 5 min in an ice/water slurry. A prewashed 1:1 slurry of 40 µL of anti-GFP-Trap-A beads (Chromotek gta-20) was added and incubated at 4 °C for 1 h with gentle rotation. Beads were collected by centrifugation at 2,000 g for 5 min at 4 °C and washed five times with ice-cold OHB1 containing 0.2% (w/v) Triton X-100. Immunoprecipitates were recovered using Laemmli buffer with β-mercaptoethanol, boiling for 10 min at 95 °C. Eluates were analyzed in immunoblots separately using the following primary antibodies: anti-UNC-29 (ref. 20, 1:500), anti-GFP (JL-8, 1:2,500, Clontech), anti-myc (GTX29106, 1:1,000, GeneTex). Horseradish peroxidase–conjugated goat anti-rabbit (K4002, DAKO) or goat anti-mouse (K4000, DAKO) were used as secondary antibodies at a 1:50 dilution. Detection was performed with LumiLight (Roche) reagents.

Endoglycosidase treatment in Xenopus *oocytes.* The same number of oocytes with similar currents, ranging from 1 to 10 µA, were suspended in 5 ml ice-cold oocyte homogenization buffer 2 (OHB2: 50 mM HEPES pH = 7.5, 100 mM NaCl, 50 mM KCl, 2 mM MgCl$_2$, 250 mM sucrose, 1 mM EDTA pH = 7.5, 1% Triton X-100, 2 mM PMSF, 1 µL Benzonase enzyme (Novagen) and Complete Protease Inhibitor). The suspension was homogenized by sonication, centrifuged at 15,000g for 5 min at

4 °C and resuspended by pipetting. A final centrifugation at 15,000g for 5 min at 4 °C was performed to remove cell debris, and its supernatant was immunoprecipitated with anti-GFP-Trap-A. Immunoprecipitated samples were resuspended in glycoprotein denaturing buffer (NEB). After boiling for 10 min at 90 °C, the supernatant was collected by centrifugation at 8,000g for 1 min at 4 °C. PNGase F or Endo H enzymes (NEB) and appropriate buffers were added. Samples were incubated for 1 h at 37 °C, then enzymes were heat-inactivated for 10 min at 90 °C. Finally, β-mercaptoethanol was added to 2%. Glycosidase treatment worked equally after solubilization in Laemmli buffer plus 2% β-mercaptoethanol.

Immunoprecipitation using C. elegans *extracts.* Membrane preparations from fractionated worm extracts were obtained as previously described[21]. Membrane extracts were resuspended in worm resuspension buffer 1 (WRB1: 50 mM HEPES pH = 7.5, 150 mM NaCl, 1 mM EDTA pH = 8.0, PMSF and Complete Protease Inhibitor) including 1% (w/v) Triton X-100, and incubated at 4 °C with gentle rotation for 30 min. The solution was further diluted to a final concentration of 0.2% (w/v) Triton X-100 with ice-cold WRB1. A pre-washed 1:1 slurry of 40 µL of anti-GFP-Trap-A beads was added and incubated overnight at 4 °C with gentle rotation. Beads were collected by centrifugation at 2,000g for 5 min at 4 °C and washed five times with ice-cold OHB1 containing 0.2% (w/v) Triton X-100. Immunoprecipitates were recovered using Laemmli buffer with β-mercaptoethanol, boiling for 10 min at 95 °C. Eluates were analyzed in immunoblots separately using the following primary antibodies: anti-UNC-29 (ref. 20, 1:500), anti-GFP (JL-8, 1:2,500, Clontech), anti-HA (Y11, 1:500, Santa Cruz). Horseradish-peroxidase-conjugated goat anti-rabbit (K4002, DAKO) or goat anti-mouse (K4000, DAKO) were used as secondary antibodies at a 1:50 dilution.

Statistical analysis. Data were analyzed using two-sided Student's *t*-test, except for **Figure 1** (one-way ANOVA and Tukey's HSD test as *post hoc* pairwise test) and **Figure 2g** (Kolmogorov-Smirnov test).

49. Woodhull, A.M. Ionic blockage of sodium channels in nerve. *J. Gen. Physiol.* **61**, 687–708 (1973).
50. Corey, J.L., Davidson, N., Lester, H.A., Brecha, N. & Quick, M.W. Protein kinase C modulates the activity of a cloned γ-aminobutyric acid transporter expressed in *Xenopus* oocytes via regulated subcellular redistribution of the transporter. *J. Biol. Chem.* **269**, 14759–14767 (1994).